On the Hopf (double Hopf) Bifurcations and Transitions of Two-Layer Western Boundary Currents

Chanh Kieu[a], Taylan Sengul[b], Quan Wang[a,c,*], Dongming Yan[d,]

[a]*Department of Earth and Atmospheric Sciences, Indiana University, Bloomington, IN 47405*
[b]*Department of Mathematics, Marmara University, 34722 Istanbul, Turkey*
[c]*Department of Mathematics, Sichuan University, Chengdu, 6100, P. R. China*
[d]*School of Data Sciences, Zhejiang University of Finance & Economics, Hangzhou, 310018, P. R. China*

Abstract

This study examines the instability and dynamical transitions of the two-layer western boundary currents represented by the Munk profile in the upper layer and a motionless bottom layer for a closed rectangular domain. First, a bound on the intensity of the Munk profile below which the western boundary currents are locally nonlinearly stable is provided. Second, by reducing the infinite dimensional system to a finite dimension via the center manifold reduction, non-dimensional transition numbers are derived, which determine the types of dynamical transitions both from a pair of simple complex eigenvalues as well as from a double pair of complex conjugate eigenvalues as the Reynolds number crosses a critical threshold. We show by careful numerical estimations of the transition numbers that the transitions in both cases are continuous at the critical Reynolds number. After the transition from a pair of simple complex eigenvalue, the western boundary layer currents turn into a periodic circulation, whereas a quasi-periodic or possibly a chaotic circulation emerges after the transition from a pair of double complex eigenvalues. Finally, a comparison between the transitions exhibited in one-layer and two-layer models is provided, which demonstrates the fundamental differences between the two models.

*Corresponding author
Email addresses: ckieu@indiana.edu (Chanh Kieu), taylansengul@gmail.com (Taylan Sengul), wangquan@indiana.edu (Quan Wang), dmyan@zufe.edu.cn (Dongming Yan)

Keywords: Western layer currents, Dynamic transitions, Continuous transition, Double Hopf bifurcation, Munk profile.
2010 MSC: 76D99, 76E20, 37L15, 37L99

1. Introduction

In ocean, western boundary currents (WBCs) are well known as a type of narrow, deep, and swift flowing currents that form on the west side of ocean basins due to a mechanism called western intensification. Due to the warm water associated with the WBCS, they play an important role in the understanding of the general oceanic surface circulation (GOSC), mostly by carrying warm water from the tropical region to the polar region. Among several WBCs in ocean, the Gulf stream, which is commonly referred to as *the* WBC [1, 2], intensifies along the western shores of the North Atlantic (east coast of North America) and exhibits boundary layer characteristics with an intense crowding of the streamlines. Other WBCs include the Agulhas Current [3].

A key problem in the current study of climate and oceanic dynamics is to understand the mechanisms behind the GOSC. As one of dominant modes of the GOSC, WBCs are typically examples of intense shear flows, which possess internal instabilities [4, 5, 6]. Those instabilities are generally regarded as the main mechanism leading to general circulation in the western boundary layer as discussed in [7]. Due to their importance in the understanding of the mechanism behind the GOSC, studying the instability of western boundary layer currents and predicting their periodic, quasi-periodic and even chaotic variability are therefore central themes in the oceanic dynamics. We refer to [8] for a recent comprehensive review of the study of GOSC from the perspective of dynamical systems theory.

The general model used to study the WBCs is often based on the quasi-geostrophic potential vorticity equations [7, 9, 10], which can be derived from the shallow water equations. Earlier studies of the WBC dynamics have mainly concentrated on either analytical solutions of simplified models or on purely

numerical simulations. Using a linearized ideal model, Stommel [11] showed in his seminal 1948 paper that the reason behind the western intensification of the wind-driven circulation is the variation of the Coriolis parameter with latitude. Munk in [12] proposed another linear model and found an analytical solution that represents a concentrated current, like the Gulf stream, later named as the celebrated Munk boundary layer profile. A boundary layer analysis of the nonlinear model and the subsequent numerical integration were then taken up and expanded by Veronis in [13, 14]. Early numerical investigations further suggested that for flows with Rossby number in the geophysical range, there is a critical Reynolds number below which a steady-state solution is asymptotically approached and a shear flow instability develops after the transition (see, e.g., [**?** 15, 16, 17]).

In general, there are two main types of instabilities for the WBCs. The first one is related to a steadily surface wind stress for which multiple steady-state solutions may coexist if the steadily wind force is sufficiently strong. For these solutions, the Hopf bifurcation can occur if the internal Rossby radius of deformation decreases, resulting in baroclinic instabilities [9, 18]. The second type of instability is the viscously-damped shear instability of barotropic WBCs, which was proposed as a mechanism for introducing time dependence to the general circulation by Bryan [4] and was later studied by Ierley and Young [19]. Using a family of basic velocity profiles and numerically solving the associated Orr-Sommerfeld equation, they found that the barotropic western boundary layer currents have viscous instabilities at comparatively low Reynolds numbers and the instabilities are not always confined within the boundary layer jet. To shed further light into the instability of WBCs, following Ierley and Young [19], Berloff and Meacham [7] studied the instability of WBCs using a simplified Munk profile in both one-layer and two-layer stratified ocean models. Their numerical results showed that the Munk profile is linearly unstable if the Reynolds number crosses a critical value, and there exists a supercritical Hopf bifurcation such that the amplitude of the bifurcated limit cycle tends to zero as the critical number is approached from the unstable side.

These previous works on the instabilities of the WBCs and the resulting formation of periodic vortices are more or less limited by the scope of the numerical investigation in the presence of multiple control parameters, which may not describe the specific details of the transition from one state to another, and so do not fully describe the physical structure of new states. Recent progress in the transition dynamics pioneered by the works of Ma and Wang [20] offer a new framework to tackle the instability of WBCs from a different angle. The main philosophy of the dynamic transition theory is to search for the full set of transition states, giving a complete characterization of the stability and transitions between two states. Within Ma and Wang's framework, phase transitions can be classified into three types: continuous, catastrophic, and random. Roughly speaking, in a continuous transition, the basic state bifurcates to a local attractor; in a catastrophic transition, the system jumps to another state, and a random transition indicates that both continuous and catastrophic transitions are possible depending on the initial perturbation. Given the advantages of the dynamic transition theory that can offer a more complete description of the transitions between different states, this theory has been successfully applied in the study of a number of transition problems, including transitions of quasi-geostrophic channel flows [21], instability and transitions of Rayleigh-Bénard convection [22, 23, 24], dynamic transitions of the Cahn-Hilliard equation [25, 26], boundary layer separation [27], as well as other problems in geophysical fluid dynamics [28, 29].

In this study, we wish to examine the stability and transitions of the WBCs in a two-layer model where the upper layer is represented by the Munk boundary layer profile and the lower layer is motionless. We first provide an upper bound on the intensity of the steady flow below which the basic solution is globally nonlinearly stable. Next, we investigate the transitions of the basic solution as the Reynolds number crosses a critical value, and numerically demonstrate that at the critical Reynolds number, a pair of simple complex conjugate eigenvalues become critical. For this case, we also prove that the transition is either continuous or catastrophic described by a Hopf bifurcation depending on the sign of a

single non-dimensional transition number. Our numerical results agree with the previous modeling studies [7, 9, 18], thus showing that the system exhibits only super-critical Hopf bifurcations, i.e., there exists a stable time-periodic solution corresponding to the periodic circulation of the WBCs.

In addition to Hopf bifurcation issue, we also tackle the problem of critical crossing of a double pair of complex eigenvalues for the first time from a dynamic transition theory point of view. This type of transition is non-generic and occurs when the control parameter crosses a codimension two critical point, which is only possible in multi parameter systems such as the one considered here. Such a critical point lies at the transversal intersection of two neutral stability curves of Hopf bifurcations and is known as double Hopf (or Hopf-Hopf) bifurcation in the bifurcation theory literature. In this case, there are many possible and very interesting transition scenarios depending on the relations between four nondimensional transition parameters, which in turn depends on the nonlinear interactions of the critical modes with the stable modes. Our numerical experiments suggest that the system admits only two possible transition scenarios and both are continuous type transitions as in the (single) Hopf case. Moreover, we prove that an S^3-attractor bifurcates when this co-dimension two critical point is crossed in the parameter space. Under the restricted parameter regime dictated by our numerical observations, we show that the bifurcated attractor has either a limit cycle or an invariant torus as a minimal attractor. When the minimal attractor is an invariant torus, the system will tend to a quasi-periodic solution whose orbit, generically, will be dense in a 2-torus.

Our final aim in this present study is to offer a comparison between the transition of the Munk profile in the one-layer and the two-layer stratified ocean models. Our results show that the abrupt transitions are possible for circulation associated with one-layer WBCs for large stratification numbers while the circulation related to two-layer WBCs always occur gradually.

The rest of this paper is organized as follows. In Section 2, the governing equations, the basic flow, and the functional setting of the problem are introduced. Section 3 presents details of the associated linear stability analysis and

nonlinear stability analysis of the basic flow, and analysis of the Principle of Exchange of Stability (PES) condition. The main results on the transitions of the basic flow and proofs are presented in Sections 4 and 5. The numerical results and physical conclusions are finally summarized in Section 6.

2. Governing Equations

A two-layer model for WBCs derived from the continuously stratified quasi-geostrophic potential vorticity equations, which is based on the Galerkin truncation mode [30, 7], is given by

$$\begin{aligned}\frac{\partial}{\partial t}\left(\Delta\psi_1 - \frac{1}{(1+\gamma)R_d^2}(\psi_1-\psi_2)\right) + J(\psi_1, \Delta\psi_1 + \frac{1}{(1+\gamma)R_d^2}\psi_2) \\ + \beta_0\frac{\partial\psi_1}{\partial x} = \nu\Delta^2\psi_1 + F(x),\end{aligned} \tag{2.1}$$

$$\begin{aligned}\frac{\partial}{\partial t}\left(\Delta\psi_2 - \frac{\gamma}{(1+\gamma)R_d^2}(\psi_2-\psi_1)\right) + J(\psi_2, \Delta\psi_2 + \frac{\gamma}{(1+\gamma)R_d^2}\psi_1) \\ + \beta_0\frac{\partial\psi_2}{\partial x} = \nu\Delta^2\psi_2,\end{aligned} \tag{2.2}$$

where $H_1(H_2)$ is the upper (lower) layer mean depth, $\gamma = \frac{H_1}{H_2}$ is the layer depth ratio, ν is the eddy viscosity coefficient, f_0 is the Coriolis parameter, β_0 is the variation of the Coriolis parameter, $F(x)$ is the surface force associated with the surface wind stress at the ocean surface, $J(f,g) = \partial_x f\partial_y g - \partial_y f\partial_x g$ is the advection operator, and Δ is the Laplacian operator. Note that the parameter $R_d = \left(\sqrt{g'}/f_0\right)\sqrt{H_1H_2/(H_1+H_2)}$ denotes here the deformation radius in two layer model, where g' is the reduced gravity. As always, the external forcing $F(x)$ related to surface wind stress is applied only to the upper layer.

To be specific, the governing equation for the WBCs is defined in a rectangular domain as follows

$$(x,y) \in \Omega = (0, L_x) \times (0, L_y),$$

where x, y denote the dimensions in the west-east and south-north directions, respectively. Let

$$(\Psi_{s1}(x), \Psi_{s2}(x)) = (\Psi_0\psi_s(x), 0)$$

be a steady state of the governing equation (2.1) where Ψ_0 is the scale of Ψ_s. Once ψ_s or the external forcing is specified, then the other can be automatically chosen to ensure the relationship

$$\beta_0 \frac{\partial \psi_s}{\partial x} = \nu \frac{\partial^4 \psi_s}{\partial x^4} + \frac{1}{\Psi_0} F(x).$$

We denote the deviation for the steady-state $(\Psi_{s1}, 0)$ as (ψ_1', ψ_2'). Upon putting $\psi_1 = \psi_1' + \Psi_{s1}$ and $\psi_2 = \psi_2'$ into the equations (2.1)–(2.2) and omitting the prime, the perturbation equations are given by

$$\begin{aligned} \frac{\partial}{\partial t}\left(\Delta\psi_1 - \frac{1}{(1+\gamma)R_d^2}(\psi_1 - \psi_2)\right) &= \nu\Delta^2\psi_1 - \beta_0\frac{\partial \psi_1}{\partial x} - J(\psi_1, \Delta\Psi_{s1}) \\ &- J(\psi_1, \Delta\psi_1 + \frac{1}{(1+\gamma)R_d^2}\psi_2) - J(\Psi_{s1}, \Delta\psi_1 + \frac{1}{(1+\gamma)R_d^2}\psi_2), \end{aligned} \tag{2.3}$$

$$\begin{aligned} \frac{\partial}{\partial t}\left(\Delta\psi_2 - \frac{\gamma}{(1+\gamma)R_d^2}(\psi_2 - \psi_1)\right) &= \nu\Delta^2\psi_2 - \beta_0\frac{\partial \psi_2}{\partial x} \\ &- J(\psi_2, \Delta\psi_2 + \frac{\gamma}{(1+\gamma)R_d^2}\psi_1) - J(\psi_2, \frac{\gamma}{(1+\gamma)R_d^2}\Psi_{s1}). \end{aligned} \tag{2.4}$$

Using $\Psi_0, (\nu/\beta_0)^{\frac{1}{3}}, \Psi_0 (\beta_0/\nu)^{\frac{1}{3}}$ and $(\nu/\beta_0)^{\frac{2}{3}}/\Psi_0$ as the scales for the stream-function, length, velocity and time, respectively, the nondimensional form of the perturbation equations (2.3)–(2.4) becomes

$$\begin{aligned} \frac{\partial}{\partial t}\left(\Delta\psi_1 - \frac{S}{1+\gamma}(\psi_1 - \psi_2)\right) &= \frac{1}{\mathrm{R}}\Delta^2\psi_1 - \frac{1}{\mathrm{R}}\frac{\partial \psi_1}{\partial x} - J(\psi_1, \Delta\psi_s) \\ &- J(\psi_s, \Delta\psi_1 + \frac{S}{1+\gamma}\psi_2) - J(\psi_1, \Delta\psi_1 + \frac{S}{1+\gamma}\psi_2), \end{aligned} \tag{2.5}$$

$$\begin{aligned} \frac{\partial}{\partial t}\left(\Delta\psi_2 - \frac{S\gamma}{1+\gamma}(\psi_2 - \psi_1)\right) &= \frac{1}{\mathrm{R}}\Delta^2\psi_2 - \frac{1}{\mathrm{R}}\frac{\partial \psi_2}{\partial x} \\ &- J(\psi_2, \Delta\psi_2 + \frac{S\gamma}{1+\gamma}\psi_1) - J(\psi_2, \frac{S\gamma}{1+\gamma}\psi_s), \end{aligned} \tag{2.6}$$

where $\mathrm{R} = \Psi_0/\nu$ is the Reynolds number, and $S = (\nu/\beta_0)^{\frac{2}{3}}/R_d^2$ is a measure of stratification. The nondimensional spatial domain for (2.5)–(2.6) is then given by

$$\Omega = \{(x, y) \mid x \in (0, a), y \in (0, b)\},$$

where

$$a = \sqrt[3]{\frac{\beta_0 L_x^3}{\nu}}, \qquad b = \sqrt[3]{\frac{\beta_0 L_y^3}{\nu}}.$$

Regarding the boundary conditions for the above perturbation equations for WBCs, it is appropriate to apply the no-slip and no-through boundary conditions in the x-direction, and the periodic boundary in the y-direction, i.e. for $i = 1, 2$,

$$\begin{aligned} &\psi_i(x, y) = \psi_i(x, y + b), \\ &\psi_i(0, y) = \psi_i(a, y) = \frac{\partial \psi_i(0, y)}{\partial x} = \frac{\partial \psi_i(a, y)}{\partial x} = 0. \end{aligned} \tag{2.7}$$

In real ocean currents, the typical value for a is $a = 50$ as in [7] so that $50/b$ is the aspect ratio of the domain Ω. With those boundary conditions and domain, we are specifically interested in the dynamical transitions of the so-called Munk profile for the mean flow ψ_s given by (see, e.g., [7])

$$\begin{aligned} v_s = \frac{d\psi_s}{dx} &= \frac{d}{dx}\left(-\frac{1}{2} e^{-x/2} \sin \frac{\sqrt{3}}{2} x - \frac{\sqrt{3}}{2} e^{-x/2} \cos \frac{\sqrt{3}}{2} x \right) \\ &= e^{-x/2} \sin \frac{\sqrt{3}}{2} x. \end{aligned} \tag{2.8}$$

2.1. Abstract form of governing equation

Let $H^4(\Omega)$, $H^2(\Omega)$, and $L^2(\Omega)$ denote the usual Sobolev and Lebesgue spaces and define H_1, H_0, and H_{-1} to be the Hilbert spaces

$$\begin{aligned} H_1 &= \{\psi = (\psi_1, \psi_2) \in H^4(\Omega) \times H^4(\Omega) |\ \psi \text{ satisfies (2.7)}\}, \\ H_0 &= \{\psi = (\psi_1, \psi_2) \in H^2(\Omega) \times H^2(\Omega) |\ \psi \text{ satisfies (2.7)}\}, \\ H_{-1} &= L^2(\Omega)^2, \end{aligned}$$

endowed with their natural inner products. We then introduce the differential operators $L, G : H_1 \to H_{-1}$ and $A : H_0 \to H_{-1}$ acting on $\psi = (\psi_1, \psi_2)$ as follows.

$$A\psi = \begin{pmatrix} \Delta\psi_1 - \frac{S}{1+\gamma}(\psi_1 - \psi_2) \\ \Delta\psi_2 - \frac{S\gamma}{1+\gamma}(\psi_2 - \psi_1) \end{pmatrix}, \tag{2.9}$$

$$L\psi = \begin{pmatrix} \frac{1}{\mathrm{R}}\Delta^2\psi_1 - \frac{1}{\mathrm{R}}\frac{\partial\psi_1}{\partial x} - J(\psi_1, \Delta\psi_s) - J(\psi_s, \Delta\psi_1 + \frac{S}{1+\gamma}\psi_2) \\ \\ \frac{1}{\mathrm{R}}\Delta^2\psi_2 - \frac{1}{\mathrm{R}}\frac{\partial\psi_2}{\partial x} - J(\psi_2, \frac{S\gamma}{1+\gamma}\psi_s) \end{pmatrix}, \tag{2.10}$$

$$G(\psi) = \begin{pmatrix} -J(\psi_1, \Delta\psi_1 + \frac{S}{1+\gamma}\psi_2) \\ \\ -J(\psi_2, \Delta\psi_2 + \frac{S\gamma}{1+\gamma}\psi_1) \end{pmatrix}.$$

By G, we also denote the following bilinear operator

$$G(\psi, \tilde{\psi}) = \begin{pmatrix} -J(\psi_1, \Delta\tilde{\psi}_1 + \frac{S}{1+\gamma}\tilde{\psi}_2) \\ \\ -J(\psi_2, \Delta\tilde{\psi}_2 + \frac{S\gamma}{1+\gamma}\tilde{\psi}_1) \end{pmatrix}, \tag{2.11}$$

defined on $H_1 \times H_1$ so that $G(\psi) = G(\psi, \psi)$.

Given those definitions, the equations (2.5)–(2.7) subject to the boundary conditions (2.7) can be put into the following abstract operator form

$$\frac{dA\psi}{dt} = L\psi + G(\psi). \tag{2.12}$$

Because of the boundary conditions (2.7), A is an isomorphism between H_0 and H_{-1}. Hence, $A^{-1} \circ L$ is a bounded operator from H_1 into H_0. Furthermore, due to the classical Sobolev embeddings, the inclusion $H_1 \hookrightarrow H_0$ is dense and compact, and thus $A^{-1} \circ L : \ D(A^{-1} \circ L) = H_1 \subset H_0 \to H_0$ has a compact resolvent.

3. Stability Analysis

3.1. Linear Analysis and the PES Condition

To study the dynamical transitions of (2.12), the first step is to verify its PES condition. For this, let's consider first the eigenvalue problem

$$L\psi = \lambda A\psi \tag{3.1}$$

and the related dual eigenvalue problem

$$L^*\psi^* = \lambda A\psi^*$$

in which L^* is the adjoint operator of L defined by

$$\langle L\psi, \varphi\rangle = \langle \psi, L^*\varphi\rangle$$

where $\langle\cdot,\cdot\rangle$ denotes the usual $L^2(\Omega)$ inner product. Apparently, the operator L is a completely continuous field, which has countably many eigenvalues.

Due to the periodicity of the problem (3.1) in the y-direction, we look for solutions of (3.1) of the form

$$\psi_m(x,y) = \exp(im\alpha y)\varphi_m(x), \qquad m \in \mathbb{Z}, \tag{3.2}$$

where

$$\alpha = 2\pi/b.$$

Upon inserting the ansatz (3.2) into (3.1), we obtain an ODE eigenvalue problem for each $m \in \mathbb{Z}$,

$$L_m\varphi_{m,k} = \lambda_{m,k}A_m\varphi_{m,k}, \qquad \varphi_{m,k} = (\varphi_{m,k,1}, \varphi_{m,k,2})^T, \tag{3.3}$$

with eigenpairs for each $k \in \mathbb{Z}_+$, where k is the order of eigenvalues for each m. For $\varphi = (\varphi_1, \varphi_2)$, the above operators are defined as

$$\begin{aligned}
&L_m = L_m^1 + L_m^2, \qquad \varphi = (\varphi_1, \varphi_2)^T,\\
&L_m^1\varphi = \frac{1}{\mathrm{R}}\begin{pmatrix} \left(D^4 - 2m^2\alpha^2D^2 + m^4\alpha^4\right)\varphi_1 - D\varphi_1 \\ \left(D^4 - 2m^2\alpha^2D^2 + m^4\alpha^4\right)\varphi_2 - D\varphi_2 \end{pmatrix},\\
&L_m^2\varphi = im\alpha\begin{pmatrix} \frac{d^3\psi_s}{dx^3}\varphi_1 - \frac{d\psi_s}{dx}\left(D^2 - m^2\alpha^2\right)\varphi_1 - \frac{S}{1+\gamma}\frac{d\psi_s}{dx}\varphi_2 \\ \frac{S\gamma}{1+\gamma}\frac{d\psi_s}{dx}\varphi_2 \end{pmatrix},\\
&A_m\varphi = \begin{pmatrix} D^2\varphi_1 - m^2\alpha^2\varphi_1 - \frac{S}{1+\gamma}(\varphi_1 - \varphi_2) \\ D^2\varphi_2 - m^2\alpha^2\varphi_2 - \frac{S\gamma}{1+\gamma}(\varphi_2 - \varphi_1) \end{pmatrix}, \quad D = \frac{d}{dx}.
\end{aligned} \tag{3.4}$$

Without loss of generality we assume that the eigenvalues of (3.3) are ordered by decreasing real part as

$$\operatorname{Re}\lambda_{m,1} \geq \operatorname{Re}\lambda_{m,2} \geq \cdots \to -\infty, \qquad \forall m \in \mathbb{Z}.$$

Assumption 3.1 (Principle of Exchange of Stabilities). *There exists a positive integer n and a critical Reynolds number $R^* > 0$ such that, for all R sufficiently close to R^*, either the condition*

$$\begin{aligned} &\operatorname{Re}\lambda_{n,1} = \operatorname{Re}\lambda_{-n,1} \begin{cases} > 0 & \text{if } R > R^*, \\ = 0 & \text{if } R = R^*, \\ < 0 & \text{if } R < R^*, \end{cases} \\ &\operatorname{Re}\lambda_{m,k} < 0 \quad \text{if } (m,k) \neq (n,1), \end{aligned} \tag{3.5}$$

or the condition

$$\begin{aligned} &\operatorname{Re}\lambda_{m,1} = \operatorname{Re}\lambda_{-m,1} \begin{cases} > 0 & \text{if } R > R^*, \\ = 0 & \text{if } R = R^*, \quad \text{for } m = n, n+1 \\ < 0 & \text{if } R < R^*, \end{cases} \\ &\operatorname{Re}\lambda_{m,k} < 0 \quad \text{if } (m,k) \neq (n,1) \text{ and } (m,k) \neq (n+1,1). \end{aligned} \tag{3.6}$$

must hold true.

For fixed parameters S, γ, b and $m \in \mathbb{Z}$, by solving $\operatorname{Re}\lambda_{m,1}(\mathrm{R}) = 0$ we obtain a unique Reynolds number $\mathrm{R}^*_m = \mathrm{R}^*_m(b, S, \gamma)$, which determines the linear stability threshold for the eigenmode $\psi_{m,1}$. In Figure 3.1, we show a typical variation of R^*_m with respect to b as numerically obtained. For fixed S and γ, we expect and observe from numerics that except for countably many values of b, there is only one $n \in \mathbb{Z}_+$ for which

$$\mathrm{R}^* = \mathrm{R}^*_n = \min_{m \in \mathbb{N}} \mathrm{R}^*_m,$$

i.e., the generic condition (3.5) holds. This defines a continuous function $\mathrm{R}^* = \mathrm{R}^*(b)$ that is piecewise smooth, with countably many cusp points at which the non-generic condition (3.6) holds. $\mathrm{R}^*(b)$ is shown in Figure 3.2.

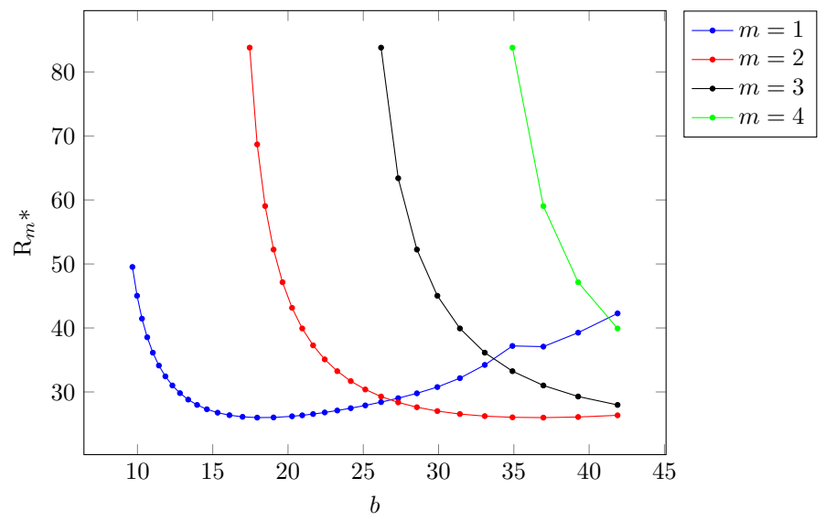

Figure 3.1: The stability curves $\mathrm{R}_m^*(b)$ for which $\mathrm{Re}\,\lambda_{m,1} = 0$ with $\gamma = 1/9$, $a = 50$, $S = 0.0457$ and for $m = 1, 2, 3, 4$.

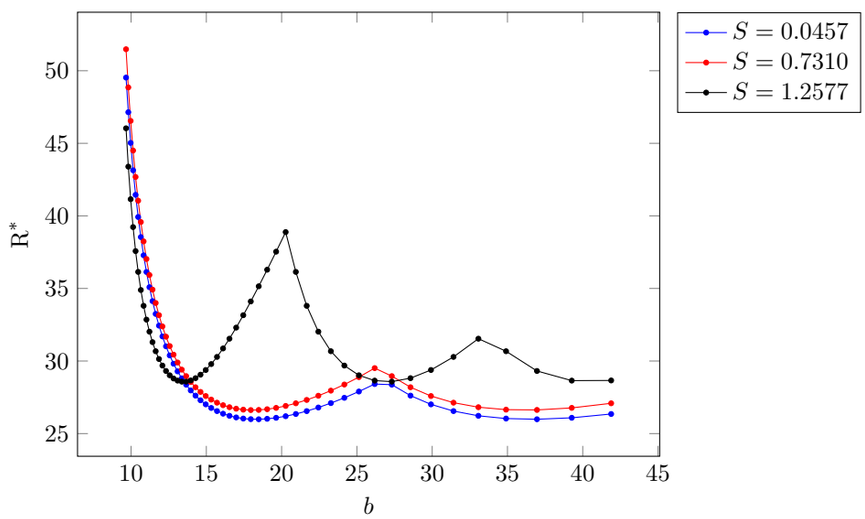

Figure 3.2: Marginal stability curves for $\gamma = 1/9$ and $a = 50$.

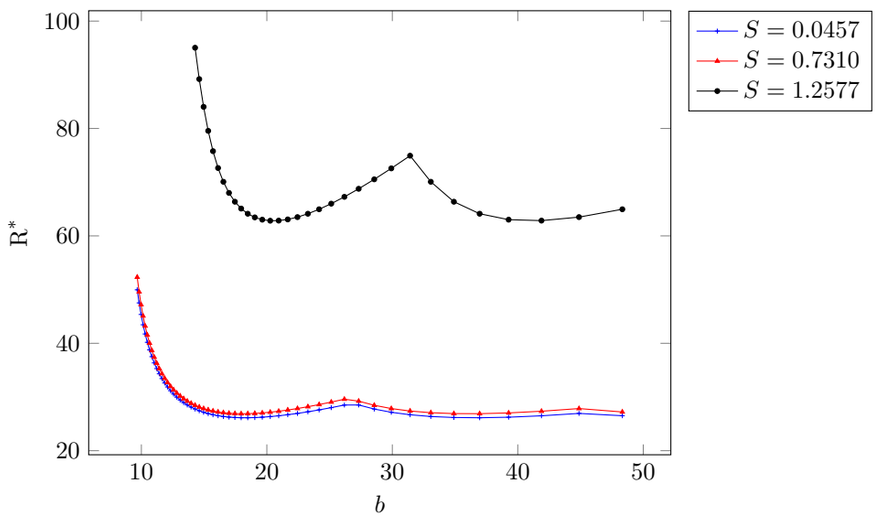

Figure 3.3: Marginal stability curves for $\gamma = 0$ and $a = 50$.

If $\gamma = 0$ in (2.5)–(2.7), then (2.5)–(2.7) is essentially a single layer model. Figure 3.2-Figure 3.3 show that the parameter γ has a prominent influence on the critical Reynolds number.

3.2. A sufficient condition for the non-linear stability

In this section, we prove a condition that guarantees the nonlinear stability of the basic solution. Our result is valid for a general steady state v_s of equations (2.5)–(2.7), which is not limited to the Munk profile. To do this, we prove first the linear stability of the basic solution by showing that the spectrum of the linear operator is in the left half of the complex plane bounded away from the imaginary axis under a given condition. Since the linear operator is also sectorial, Theorem 5.1.1 in [31] shows then that the linear stability of the basic solution also implies the locally nonlinear stability. Let's denote by $\|v_s\|_\infty$ the L^∞-norm of the steady state profile, we have the following theorem

Theorem 3.1. *For any $m \in \mathbb{Z}\setminus\{0\}$ and any $k \in \mathbb{Z}_+$, the eigenvalue* $\operatorname{Re}\lambda_{m,k} <$

0 *if*

$$R \leq \frac{2|m|^3\alpha^3(1+\gamma)}{\|v_s\|_\infty \sqrt{m^4\alpha^4(1+\gamma)^2+S^2\gamma}}. \tag{3.7}$$

For any $k \in \mathbb{Z}_+$ *and for any Reynolds number, the eigenvalue* $\operatorname{Re}\lambda_{0,k} < 0$. *Moreover if the condition* (3.7) *is true for the critical wave integer* $m = n$ *in Assumption 3.1, then the zero solution of* (2.12) *is locally nonlinearly stable.*

Proof 3.1. *Let* $m \in \mathbb{Z}$, *and suppose that* $\varphi_{m,1}$ *is the eigenvector corresponding to the eigenvalue* $\lambda_{m,1}$ *of* (3.3) *with largest real part. Let us set,*

$$\varphi = (\varphi_1, \varphi_2) = \varphi_{m,1} = (\varphi_{m,1,1}, \varphi_{m,1,2})$$

throughout this proof. Also by $\|\cdot\|$, *we denote the usual* L^2 *norm on the interval* $(0, a)$. *A straightforward calculation of the identity*

$$(L_m\varphi, \varphi) = \lambda_{m,1}\left(A_m\varphi, \varphi\right),$$

gives the following relations

$$\begin{aligned}
&\|\varphi_1''\|^2 + 2m^2\alpha^2\|\varphi_1'\|^2 - iRm\alpha\int_0^a v_s\varphi_1''\overline{\varphi_1}dx \\
&- \int_0^a \varphi_1'\overline{\varphi_1}dx + m^4\alpha^4\|\varphi_1\|^2 + iRm^3\alpha^3\int_0^a v_s|\varphi_1|^2dx \\
&+ iRm\alpha\int_0^a v_s''|\varphi_1|^2dx - \frac{iRm\alpha S}{1+\gamma}\int_0^a v_s\varphi_2\overline{\varphi_1}dx \\
&= -\lambda_{m,1}R\left(\|\varphi_1'\|^2 + \frac{m^2\alpha^2(1+\gamma)+S}{1+\gamma}\|\varphi_1\|^2 - \frac{S}{1+\gamma}\int_0^a \varphi_2\overline{\varphi_1}dx\right),
\end{aligned} \tag{3.8}$$

and

$$\begin{aligned}
&\|\varphi_2''\|^2 + 2m^2\alpha^2\|\varphi_2'\|^2 - \int_0^a \varphi_2'\overline{\varphi_2}dx + m^4\alpha^4\|\varphi_2\|^2 + \frac{iRm\alpha S\gamma}{1+\gamma}\int_0^a v_s\varphi_2\overline{\varphi_2}dx \\
&= -\lambda_{m,1}R\left(\|\varphi_2'\|^2 + \frac{m^2\alpha^2(1+\gamma)+S\gamma}{1+\gamma}\|\varphi_2\|^2 - \frac{S\gamma}{1+\gamma}\int_0^a \varphi_1\overline{\varphi_2}dx\right).
\end{aligned} \tag{3.9}$$

Using the fact,

$$\operatorname{Re}\int_0^a \varphi_i'\overline{\varphi_i}dx = \frac{1}{2}\int_0^a \frac{d}{dx}|\varphi_i|^2dx = 0, \qquad i = 1, 2,$$

as a result of the imposed boundary conditions, and considering the real part of $\gamma\times$ (3.8) + (3.9), *we obtain*

$$I_1 = -R\operatorname{Re}\left(\lambda_{m,1}I_2\right), \tag{3.10}$$

where

$$\begin{aligned}
I_1 =&\gamma\left(\|\varphi_1''\|^2+2m^2\alpha^2\|\varphi_1'\|^2+m^4\alpha^4\|\varphi_1\|^2\right)\\
&+\left(\|\varphi_2''\|^2+2m^2\alpha^2\|\varphi_2'\|^2+m^4\alpha^4\|\varphi_2\|^2\right)\\
&+Rm\alpha\gamma I_3,\\
I_2 =&\gamma\|\varphi_1'\|^2+m^2\alpha^2\gamma\|\varphi_1\|^2+\|\varphi_2'\|^2+m^2\alpha^2\|\varphi_2\|^2\\
&+\frac{S\gamma}{1+\gamma}\left(\|\varphi_1\|^2+\|\varphi_2\|^2-\int_0^a(\varphi_2\overline{\varphi_1}+\varphi_1\overline{\varphi_2})dx\right),\\
I_3 =&-\operatorname{Re}\left(i\int_0^a v_s\varphi_1''\overline{\varphi_1}dx+\frac{iS}{1+\gamma}\int_0^a v_s\varphi_2\overline{\varphi_1}dx\right).
\end{aligned}$$

It is easy to see that I_2 is real and in fact positive. Hence (3.10) implies that

$$\operatorname{Re}(\lambda_{m,1})<0 \iff I_1>0. \tag{3.11}$$

This is automatically satisfied for $m=0$. Now assume $m\in\mathbb{Z}\setminus\{0\}$. With the estimate

$$I_3\geq-\|v_s\|_\infty\left(\frac{\varepsilon_1\|\varphi_1''\|^2}{2}+\frac{\|\varphi_1\|^2}{2\varepsilon_1}+\frac{S}{1+\gamma}\frac{\varepsilon_2\|\varphi_2\|^2}{2}+\frac{S}{1+\gamma}\frac{\|\varphi_1\|^2}{2\varepsilon_2}\right)$$

where ε_1 and ε_2 are chosen as

$$\varepsilon_1=\frac{2}{Rm\alpha\|v_s\|_\infty},\qquad \varepsilon_2=\frac{2m^3\alpha^3(1+\gamma)}{RS\gamma\|v_s\|_\infty},$$

so that the first two terms in the below estimate are zero, we obtain

$$\begin{aligned}
I_1>&\left(\gamma-Rm\alpha\gamma\|v_s\|_\infty\frac{\varepsilon_1}{2}\right)\|\varphi_1''\|^2+\left(m^4\alpha^4-\frac{Rm\alpha S\gamma\|v_s\|_\infty}{1+\gamma}\frac{\varepsilon_2}{2}\right)\|\varphi_2\|^2\\
&+\left(\gamma m^4\alpha^4-\frac{Rm\alpha\gamma\|v_s\|_\infty}{2\varepsilon_1}-\frac{Rm\alpha S\gamma\|v_s\|_\infty}{2\varepsilon_2(1+\gamma)}\right)\|\varphi_1\|^2\\
\geq&\left(\gamma m^4\alpha^4-\frac{R^2m^2\alpha^2\gamma\|v_s\|_\infty^2}{4}-\frac{R^2S^2\gamma^2\|v_s\|_\infty^2}{4m^2\alpha^2(1+\gamma)^2}\right)\|\varphi_1\|^2.
\end{aligned}$$

Now the condition (3.7) implies that $I_1>0$ hence $\operatorname{Re}(\lambda_{m,1})<0$ by (3.11) which finishes the proof.

Remark 3.1. *The L^∞ norm of the Munk profile (i.e. its maximum velocity) (2.8) can be computed exactly as*

$$\|v_s\|_\infty=\frac{\sqrt{3}}{2}e^{-\frac{\sqrt{3}\pi}{9}}=0.4731.$$

Remark 3.2. *Theorem 3.1 also partially justifies Assumption 3.1. For fixed parameters R, S, γ and α, there must exist $N \in \mathbb{Z}_+$ such that the condition (3.7) is satisfied. Hence* $\operatorname{Re}\lambda_{m,1} < 0$ *for all integers m with $|m| \geq N$.*

4. Main Transition Theorems

In this section, we present the first dynamic transitions associated with the equations (2.5)–(2.7). To describe the solutions that bifurcate from the basic steady state (Munk profile), we define the following time periodic functions

$$f_m(x,y,t) = 2\operatorname{Re}\left(\exp\left(i\operatorname{Im}(\lambda_{m,1})t + im\alpha y\right)\varphi_{m,1}(x)\right), \quad m \in \mathbb{Z} \tag{4.1}$$

where $\lambda_{m,1}$ is the first eigenvalue of (3.3) and $\varphi_{m,1}$ is its associated eigenfunction.

Lemma 4.1. *Assume that the first critical eigenvalue is complex simple so that the assumption (3.5) holds. Then the transition and stability of the steady state solution (2.8) for the equations (2.5)–(2.7) in the vicinity of the critical Reynolds number $R = R^*$ and for any sufficiently small initial condition are equivalent to the stability of the zero solution of the equation*

$$\frac{d\eta}{dt} = \lambda_{n,1}\eta + P\eta|\eta|^2 + o(|\eta|^3). \tag{4.2}$$

where $\eta(t) \in \mathbb{C}$ denotes the amplitude of the projection of the solution onto the first eigenvector and the ***transition number*** *$P \in \mathbb{C}$ is determined by the nonlinear interactions of the first eigenvector and its dual eigenvector, given by (5.11).*

The analysis of Lemma 4.1 yields the following theorem.

Theorem 4.1. *Assume that the first critical eigenvalue has simple complex multiplicity and the condition (3.5) is satisfied. Then the following assertions hold true.*

(1) If $\operatorname{Re}(P) < 0$*, the system (2.5)–(2.7) undergoes a continuous transition accompanied by a supercritical Hopf bifurcation on $R > R^*$. In particular,*

the steady-state solution $\mathbf{0}$ *bifurcates to a stable periodic solution* ψ *on* $R > R^*$*, satisfying* $\psi \to \mathbf{0}$ *as* $R \to R^{*+}$ *and has the following approximation*

$$\psi(x,y,t) = \left(\frac{-\operatorname{Re}(\lambda_{n,1})}{\operatorname{Re}(P)}\right)^{\frac{1}{2}} f_n(x,y,t) + o\left(|\operatorname{Re}(\lambda_{n,1})|\right)^{\frac{1}{2}}. \tag{4.3}$$

instead of

$$\psi(x,y,t) = \left(\frac{\operatorname{Re}(\lambda_{n,1})}{|\operatorname{Re}(P)|}\right)^{\frac{1}{2}} f_n(x,y,t) + o\left(\operatorname{Re}(\lambda_{n,1})\right)^{\frac{1}{2}}.$$

so that the formula is also true for (2).

(2) If $\operatorname{Re}(P) > 0$*, the system* (2.5)–(2.7) *undergoes a jump transition on* $R < R^*$ *accompanied by a subcritical Hopf bifurcation. In particular, an unstable periodic orbit* ψ *given by* (4.3) *bifurcates on* $R < R^*$ *such that* $\psi \to 0$ *as* $R \to R^{*-}$*, and there is no periodic solution bifurcating from* $\mathbf{0}$ *on* $R > R^*$*. Moreover, there is a singularity separation at some* $R_s < R^*$ *generating an attractor and an unstable periodic orbit* ψ*.*

We now consider the case of a double pair of complex conjugate eigenvalues becoming critical at the critical Reynolds number. We first present the reduced equations in this case.

Lemma 4.2. *Assume that the first critical eigenvalues have complex multiplicity 2 so that the assumption* (3.6) *holds. Then, the transition and stability of the steady state solution* (2.8) *of the equations* (2.5)–(2.7) *in the vicinity of the critical Reynolds number* $R = R^*$ *and for any sufficiently small initial condition are equivalent to the stability of the zero solution of the following equations*

$$\begin{aligned} \frac{\partial \eta_1}{\partial t} &= \lambda_{n,1}\eta_1 + \eta_1(A|\eta_1|^2 + B|\eta_2|^2) + o(|\eta_1| + |\eta_2|)^3), \\ \frac{\partial \eta_2}{\partial t} &= \lambda_{n+1,1}\eta_2 + \eta_2(C|\eta_1|^2 + D|\eta_2|^2) + o(|\eta_1| + |\eta_2|)^3), \end{aligned} \tag{4.4}$$

where $\eta_1(t), \eta_2(t) \in \mathbb{C}$ *denote the amplitudes of the projection of the solution onto the first eigenvectors and the* ***transition numbers*** A, B, C, D *are determined by the nonlinear interactions of the first eigenvectors and their dual eigenvectors given by* (5.20).

To present the transition theorem related to the analysis of the equations (4.4), we define the following parameters.

$$\theta = \frac{\mathrm{Re}(B)}{\mathrm{Re}(D)}, \quad \delta = \frac{\mathrm{Re}(C)}{\mathrm{Re}(A)}. \tag{4.5}$$

It is known that (see [32]) the system (4.4) exhibits many interesting dynamic behaviors depending on these coefficients. Here, we restrict our attention to the case

$$\mathrm{Re}(A) < 0, \quad \mathrm{Re}(D) < 0, \quad \theta < 0, \quad \delta > 0 \tag{4.6}$$

which is the only case we observe in our numerical experiments. For the next theorem, let us define the solutions

$$\begin{aligned}
\psi_{P1}(x,y,t) &= \left(\frac{\mathrm{Re}(\lambda_{n,1})}{|\mathrm{Re}(A)|}\right)^{\frac{1}{2}} f_n(x,y,t) + o\left(\mathrm{Re}(\lambda_{n,1})\right)^{\frac{1}{2}}, \\
\psi_{P2}(x,y,t) &= \left(\frac{\mathrm{Re}(\lambda_{n+1,1})}{|\mathrm{Re}(D)|}\right)^{\frac{1}{2}} f_{n+1}(x,y,t) + o\left(\mathrm{Re}(\lambda_{n+1,1})\right)^{\frac{1}{2}}, \\
\psi_{P3}(x,y,t) &= \left(\frac{\mathrm{Re}(\lambda_{n,1}) - \theta\,\mathrm{Re}(\lambda_{n+1,1}))}{(\theta\delta - 1)\,\mathrm{Re}(A)}\right)^{\frac{1}{2}} f_n(x,y,t) \\
&\quad + \left(\frac{\delta\,\mathrm{Re}(\lambda_{n,1}) - \mathrm{Re}(\lambda_{n+1,1}))}{(\theta\delta - 1)\,\mathrm{Re}(D)}\right)^{\frac{1}{2}} f_{n+1}(x,y,t) \\
&\quad + o\left(\left(|\mathrm{Re}(\lambda_{n,1})| + |\mathrm{Re}(\lambda_{n+1,1})|\right)^{\frac{1}{2}}\right).
\end{aligned}$$

Theorem 4.2. *Assume that the conditions of Lemma 4.2 as well as the condition (4.6) hold. Then the equations (2.5)–(2.7) undergo a continuous transition at $R = R^*$, and an S^3 attractor Σ bifurcates on $R > R^*$, which converges to $\mathbf{0}$ as $R \to R^{*+}$. Furthermore, the topological structure of Σ is as follows.*

1. *If $\delta\,\mathrm{Re}(\lambda_{n,1}) < \mathrm{Re}(\lambda_{n+1,1})$, Σ contains the orbits of the periodic solutions ψ_{P1} and ψ_{P2} and the orbit of the quasi-periodic solution ψ_{P3} which is an invariant torus. Moreover ψ_{P1} and ψ_{P2} are unstable while ψ_{P3} is stable and the phase portrait is as shown in Figure 4.1.*

2. *If $\delta\,\mathrm{Re}(\lambda_{n,1}) > \mathrm{Re}(\lambda_{n+1,1})$, Σ contains the orbits of the periodic solutions ψ_{P1} and ψ_{P2}. Moreover ψ_{P1} is stable while ψ_{P2} is unstable, and the phase portrait is shown in Figure 4.2.*

Remark 4.1. *If $\eta_2 = 0$ or $\eta_1 = 0$, the equations (4.4) will be reduced to (4.2) with $A = P$ or $D = P$ respectively. Thus Lemma 4.1 and Theorem 4.1 are special cases of Lemma 4.2 and Theorem 4.2 respectively.*

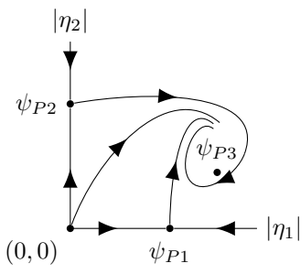

Figure 4.1: The case $\delta\,\mathrm{Re}(\lambda_{n,1}) < \mathrm{Re}(\lambda_{n+1,1})$ in Theorem 4.2.

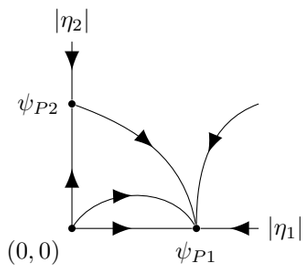

Figure 4.2: The case $\delta\,\mathrm{Re}(\lambda_{n,1}) > \mathrm{Re}(\lambda_{n+1,1})$ in Theorem 4.2.

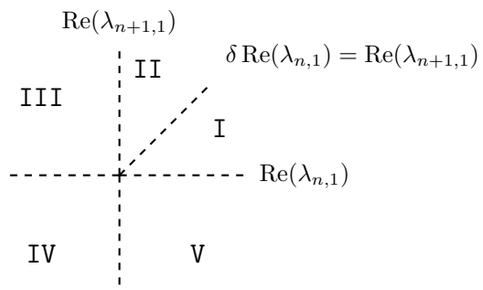

Figure 4.3: The regions in the $\mathrm{Re}(\lambda_{n,1})$–$\mathrm{Re}(\lambda_{n+1,1})$ plane with different dynamical behaviors according to Theorem 4.2. In region `IV`, the basic steady state is locally asymptotically stable, in regions `I`, `III` and `V`, the system undergoes a supercritical Hopf bifurcation. In region `II`, the system will tend to a quasi-periodic solution whose orbit is dense in a 2D torus in the phase space.

5. The proofs

5.1. Proof of Lemma 4.1

To prove the theorems stated in the previous sections, let's denote the first eigenvector and its dual eigenvector as

$$\begin{aligned} \psi_n &= \psi_{n,1} = e^{in\alpha y}\varphi_n(x), \quad \varphi_n(x) = (\varphi_{n,1}(x), \varphi_{n,2}(x)), \\ \psi_n^* &= \psi_{n,1}^* = e^{in\alpha y}\varphi_n^*(x), \quad \varphi_n^*(x) = (\varphi_{n,1}^*(x), \varphi_{n,2}^*(x)), \end{aligned} \tag{5.1}$$

respectively. Our proof will follow the center manifold reduction approach as outlined in [20]. Denote the center space as H_c which is spanned by all first eigenvectors. Any element $\phi \in H_c$ can be therefore expressed as

$$\phi = \eta\psi_n + \overline{\eta\psi_n}, \qquad \eta \in \mathbb{C}. \tag{5.2}$$

We express next the center manifold function as

$$h(\phi) = h_2(\phi) + o(|\eta|^2).$$

Then, the quadratic approximation of the center manifold function, h_2, is the solution of the linear nonhomogeneous equation

$$\begin{aligned} 2\lambda_{n,1}Ah_2(\phi) - Lh_2(\phi) = G(\phi,\phi) =& \eta^2 G(\psi_n,\psi_n) + \overline{\eta}^2 G(\overline{\psi_n},\overline{\psi_n}) \\ &+ |\eta|^2 (G(\psi_n,\overline{\psi_n}) + G(\overline{\psi_n},\psi_n)), \end{aligned} \tag{5.3}$$

where the linear operators A, L and the bilinear operator G are defined by (2.9), (2.10) and (2.11) respectively. We note that the approximation (5.3) is a special case of the approximation given later in the proof of Lemma 4.2. A direct computation yields

$$\begin{aligned} \frac{1}{e^{2in\alpha}in\alpha}G(\psi_n,\psi_n) = &\begin{pmatrix} -\frac{d\varphi_{n,1}}{dx}\left(\frac{d^2\varphi_{n,1}}{dx^2} - n^2\alpha^2\varphi_{n,1}\right) \\ -\frac{d\varphi_{n,2}}{dx}\left(\frac{d^2\varphi_{n,2}}{dx^2} - n^2\alpha^2\varphi_{n,2}\right) \end{pmatrix} + \\ &\begin{pmatrix} \varphi_{n,1}\left(\frac{d^3\varphi_{n,1}}{dx^3} - n^2\alpha^2\frac{d\varphi_{n,1}}{dx}\right) \\ \varphi_{n,2}\left(\frac{d^3\varphi_{n,2}}{dx^3} - n^2\alpha^2\frac{d\varphi_{n,2}}{dx}\right) \end{pmatrix} + \frac{S}{1+\gamma}\begin{pmatrix} -\frac{d\varphi_{n,1}}{dx}\varphi_{n,2} + \varphi_{n,1}\frac{d\varphi_{n,2}}{dx} \\ \gamma\left(-\frac{d\varphi_{n,2}}{dx}\varphi_{n,1} + \varphi_{n,2}\frac{d\varphi_{n,1}}{dx}\right) \end{pmatrix}, \end{aligned}$$

$$\frac{1}{in\alpha}G(\psi_n,\overline{\psi_n}) = \begin{pmatrix} \frac{d\varphi_{n,1}}{dx}\left(\frac{d^2\overline{\varphi_{n,1}}}{dx^2} - n^2\alpha^2\overline{\varphi_{n,1}}\right) \\ \frac{d\varphi_{n,2}}{dx}\left(\frac{d^2\overline{\varphi_{n,2}}}{dx^2} - n^2\alpha^2\overline{\varphi_{n,2}}\right) \end{pmatrix} + \begin{pmatrix} \varphi_{n,1}\left(\frac{d^3\overline{\varphi_{n,1}}}{dx^3} - n^2\alpha^2\frac{d\overline{\varphi_{n,1}}}{dx}\right) \\ \varphi_{n,2}\left(\frac{d^3\overline{\varphi_{n,1}}}{dx^3} - n^2\alpha^2\frac{d\overline{\varphi_{n,2}}}{dx}\right) \end{pmatrix} + \frac{S}{1+\gamma}\begin{pmatrix} \frac{d\varphi_{n,1}}{dx}\overline{\varphi_{n,2}} + \varphi_{n,1}\frac{d\overline{\varphi_{n,2}}}{dx} \\ \gamma\left(\frac{d\varphi_{n,2}}{dx}\overline{\varphi_{n,1}} + \varphi_{n,2}\frac{d\overline{\varphi_{n,1}}}{dx}\right) \end{pmatrix},$$

$$G(\overline{\psi_n},\overline{\psi_n}) = \overline{G(\psi_n,\psi_n)}, \qquad G(\overline{\psi_n},\psi_n) = \overline{G(\psi_n,\overline{\psi_n})}.$$

By the tangent conditions of the central manifold $h_2(0) = 0$ and $Dh_2(0) = 0$. Thus, $h_2(\phi)$ has the following expansion

$$h_2(\phi) = \eta^2\Psi_{20} + |\eta|^2\Psi_{11} + \overline{\eta}^2\Psi_{02} + o(|\eta|^2). \tag{5.4}$$

(5.3) and the above forms require that $\Psi_{20}, \Psi_{11}, \Psi_{02}$ must have a form

$$\begin{aligned} \Psi_{20} &= e^{i2n\alpha y}M_1(x), \\ \Psi_{11} &= M_2(x), \\ \Psi_{02} &= e^{-i2n\alpha y}M_3(x). \end{aligned} \tag{5.5}$$

It follows from the preceding equation and (5.3) that M_1, M_2, M_3 are determined by following equations

$$\begin{aligned} &2\lambda_{n,1}A_{2n}M_1 - L_{2n}M_1 = e^{-i2n\alpha y}G(\psi_n,\psi_n), \\ &2\overline{\lambda_{n,1}}A_{2n}M_3 - L_{2n}M_3 = e^{i2n\alpha y}G(\overline{\psi_n},\overline{\psi_n}), \\ &2\,\mathrm{Re}(\lambda_{n,1})A_0M_2 - L_0M_2 = G(\psi_n,\overline{\psi_n}) + G(\overline{\psi_n},\psi_n). \end{aligned} \tag{5.6}$$

To obtain a unique transition number, we normalize the first eigenvectors in the following manner

$$(A\psi_n,\psi_n^*)/b = 1.$$

and obtain the reduced equation as

$$\frac{d\eta}{dt} = \lambda_{n,1}\eta + (G(\phi,\phi) + G(\phi,h_2) + G(h_2,\phi),\psi_n^*) + o(|\eta|^3), \tag{5.7}$$

by the procedure explained in the proof of Lemma 4.2.

It follows from (5.2) and (5.4) that

$$\begin{aligned}(G(\phi,h_2),\psi_n^*) =& \left(G(\eta\psi_n+\overline{\eta\psi_n},\eta^2\Psi_{20}+|\eta|^2\Psi_{11}+\overline{\eta}^2\Psi_{02}),\psi_n^*\right)\\ =&\eta^3\left(G(\psi_n,\Psi_{20}),\psi_n^*\right)+\eta|\eta|^2\left(G(\overline{\psi_n},\Psi_{20}),\psi_n^*\right)\\ &+\eta|\eta|^2\left(G(\psi_n,\Psi_{11}),\psi_n^*\right)+\overline{\eta}|\eta|^2\left(G(\overline{\psi_n},\Psi_{11}),\psi_n^*\right)\\ &+\overline{\eta}|\eta|^2\left(G(\psi_n,\Psi_{02}),\psi_n^*\right)+\overline{\eta}^3\left(G(\overline{\psi_n},\Psi_{02}),\psi_n^*\right),\end{aligned} \tag{5.8}$$

$$\begin{aligned}(G(h_2,\phi),\psi_n^*) =& \left(G(\eta^2\Psi_{20}+|\eta|^2\Psi_{11}+\overline{\eta}^2\Psi_{02},\eta\psi_n+\overline{\eta\psi_n}),\psi_n^*\right)\\ =&\eta^3\left(G(\Psi_{20},\psi_n),\psi_n^*\right)+\eta|\eta|^2\left(G(\Psi_{20},\overline{\psi_n}),\psi_n^*\right)\\ &+\eta|\eta|^2\left(G(\Psi_{11},\psi_n),\psi_n^*\right)+\overline{\eta}|\eta|^2\left(G(\Psi_{11},\overline{\psi_n}),\psi_n^*\right)\\ &+\overline{\eta}|\eta|^2\left(G(\Psi_{02},\psi_n),\psi_n^*\right)+\overline{\eta}^3\left(G(\Psi_{02},\overline{\psi_n}),\psi_n^*\right),\end{aligned} \tag{5.9}$$

Using (5.1) and (5.5) we find that

$$\begin{aligned}&\left(G(\psi_n,\Psi_{20}),\psi_n^*\right)=\left(G(\Psi_{20},\psi_n),\psi_n^*\right)=0,\\ &\left(G(\overline{\psi_n},\Psi_{11}),\psi_n^*\right)=\left(G(\Psi_{11},\overline{\psi_n}),\psi_n^*\right)=0,\\ &\left(G(\psi_n,\Psi_{02}),\psi_n^*\right)=\left(G(\Psi_{02},\psi_n),\psi_n^*\right)=0,\\ &\left(G(\overline{\psi_n},\Psi_{02}),\psi_n^*\right)=\left(G(\Psi_{02},\overline{\psi_n}),\psi_n^*\right)=0.\end{aligned} \tag{5.10}$$

Finally plugging (5.8), (5.9) and (5.10) into (5.7), we obtain (4.2) where

$$\begin{aligned}P=&\left(G(\overline{\psi_n},\Psi_{20}),\psi_n^*\right)+\left(G(\psi_n,\Psi_{11}),\psi_n^*\right)\\ &+\left(G(\Psi_{20},\overline{\psi_n}),\psi_n^*\right)+\left(G(\Psi_{11},\psi_n),\psi_n^*\right),\end{aligned} \tag{5.11}$$

which finishes the proof.

5.2. Proof of Theorem 4.1

The proof of Theorem 4.1 depends on the analysis of the reduced equations (4.2), which is standard and leads to the classical Hopf bifurcation. Specifically, when $\mathrm{Re}(P)<0$, at $\mathrm{R}=\mathrm{R}^*$, 0 is a locally stable fixed point of (2.5)–(2.7). Therefore, using Theorem 2.3.5 and Theorem 2.5.4 in [20], the equations (2.5)–(2.7) bifurcate from $(\psi,R)=(0,R^*)$ to a stable periodic solution on $R>R^*$ if $\mathrm{Re}(P)<0$. Similarly, if $\mathrm{Re}(P)>0$, (2.5)–(2.7) bifurcates from $(\psi,R)=(0,R^*)$ to an unstable periodic solution on $R<R^*$.

5.3. Proof of Lemma 4.2

Let the first four critical eigenfunctions be given by

$$\begin{aligned} \psi_n &= \psi_{n,1} = e^{in\alpha y}\varphi_n(x), \qquad & \psi_{n+1} &= \psi_{n+1,1} = e^{i(n+1)\alpha y}\varphi_{n+1}(x), \\ \psi_n^* &= \psi_{n,1}^* = e^{in\alpha y}\varphi_n^*(x), \qquad & \psi_{n+1}^* &= \psi_{n+1,1}^* = e^{i(n+1)\alpha y}\varphi_{n+1}^*(x) \end{aligned} \tag{5.12}$$

along with their complex conjugates. We use the asterisks above to denote the dual eigenfunctions. We assume that the first eigenfunctions are normalized so that

$$\begin{aligned} (A\psi_n, \psi_n^*)/b &= \frac{1}{b}\int_0^a \int_0^b A\psi_n \overline{\psi_n^*} dxdy = 1, \\ (A\psi_{n+1}, \psi_{n+1}^*)/b &= \frac{1}{b}\int_0^a \int_0^b A\psi_{n+1} \overline{\psi_{n+1}^*} dxdy = 1. \end{aligned}$$

For ease of notation, we denote

$$\begin{aligned} &\psi_1' = \psi_n, \quad \psi_2' = \psi_{n+1}, \quad \psi_3' = \overline{\psi_n}, \quad \psi_4' = \overline{\psi_{n+1}} \\ &\lambda_1' = \lambda_n, \quad \lambda_2' = \lambda_{n+1}, \quad \lambda_3' = \overline{\lambda_n}, \quad \lambda_4' = \overline{\lambda_{n+1}} \\ &\varphi_1' = \varphi_n, \quad \varphi_2' = \varphi_{n+1}, \quad \varphi_3' = \overline{\varphi_n}, \quad \varphi_4' = \overline{\varphi_{n+1}} \\ &m_1 = n, \quad m_2 = n+1, \quad m_3 = -n, \quad m_4 = -n-1 \end{aligned}$$

and omit the primes. Denote the first characteristic space as H_c that is spanned by all first eigenvectors. Then, any element ϕ in H_c can be expressed as

$$\phi = \eta_1\psi_1 + \eta_2\psi_2 + \eta_3\psi_3 + \eta_4\psi_4. \tag{5.13}$$

where $\eta_1, \eta_2 \in \mathbb{C}$ and

$$\eta_3 = \overline{\eta_1}, \quad \eta_4 = \overline{\eta_2},$$

As a result, the local center manifold M_c can be described in terms of a sufficiently smooth function $h : H_c \to H = H_c^{\perp}$ such that $h(0) = 0, Dh(0) = 0$, and the local manifold M_c can be expressed by

$$M_c = \big\{\phi + h(\phi) | \phi \in H_c\big\}.$$

Clearly, the tangent conditions $h(0) = 0, Dh(0) = 0$ yield an expression for h that can be approximated by

$$h(\phi) = h_2(\phi) + o(|\eta|^2) = D^2h(0)(\phi)^2 + o(|\eta|^2).$$

On the center manifold M_c, the full PDE can be reduced to a system of ODEs by substituting $\psi = \phi + h(\phi)$ into (2.12) and taking its Riesz projection onto H_c. Explicitly, for $\phi \in H_c$ of the form (5.13), we now have

$$\frac{\partial}{\partial t}(A\phi) + \frac{\partial}{\partial t}(Ah(\phi)) = L\phi + Lh(\phi) + G(\phi + h(\phi), \phi + h(\phi)). \tag{5.14}$$

By taking the aforementioned projections, we get

$$\begin{aligned} \frac{\partial \eta_1}{\partial t} &= \lambda_1\eta_1 + \left(G(\phi + h(\phi), \phi + h(\phi)), \psi_1^*\right), \\ \frac{\partial \eta_2}{\partial t} &= \lambda_2\eta_2 + \left(G(\phi + h(\phi), \phi + h(\phi)), \psi_2^*\right). \end{aligned} \tag{5.15}$$

Now, following (5.14), we will demonstrate the explicit computation of $h_2(\phi) = D^2h(0)(\phi)^2$. First, we consider the equation

$$\frac{d}{dt}Au^1 = Lu^1, \qquad u^1(0) = \sum_{j=1}^{4} \eta_j\psi_j,$$

whose solution is given by

$$u^1(t, x, y) = \sum_{j=1}^{4} e^{\lambda_j t}\eta_j\psi_j(x, y).$$

Next we write

$$G(u^1, u^1) = \sum_{j,k=1}^{4} \eta_j\eta_k e^{(\lambda_j+\lambda_k)t} e^{i(m_j+m_k)\alpha y} G_{m_j,m_k}(\varphi_j(x), \varphi_k(x)),$$

where $G_{m,l}(\cdot, \cdot)$ is defined as

$$\begin{aligned} G_{m,n}(\varphi_m(x), \varphi_l(x)) = &\begin{pmatrix} -il\alpha \frac{d\varphi_{m,1}}{dx}\left(\frac{d^2\varphi_{l,1}}{dx^2} - l^2\alpha^2\varphi_{l,1}\right) \\ -il\alpha \frac{d\varphi_{m,2}}{dx}\left(\frac{d^2\varphi_{l,2}}{dx^2} - l^2\alpha^2\varphi_{l,2}\right) \end{pmatrix} \\ + &\begin{pmatrix} im\alpha\varphi_{m,1}\left(\frac{d^3\varphi_{l,1}}{dx^3} - l^2\alpha^2\frac{d\varphi_{l,1}}{dx}\right) \\ im\alpha\varphi_{m,2}\left(\frac{d^3\varphi_{l,2}}{dx^3} - l^2\alpha^2\frac{d\varphi_{l,2}}{dx}\right) \end{pmatrix} \end{aligned}$$

$$+\frac{S}{1+\gamma}\begin{pmatrix} -il\alpha\frac{d\varphi_{m,1}}{dx}\varphi_{l,2}+im\alpha\varphi_{m,1}\frac{d\varphi_{l,2}}{dx} \\ \gamma\left(-il\alpha\frac{d\varphi_{m,2}}{dx}\varphi_{l,1}+im\alpha\varphi_{m,2}\frac{d\varphi_{l,1}}{dx}\right)\end{pmatrix},$$

$$\varphi_m=(\varphi_{m,1},\varphi_{m,2})^T,\qquad \varphi_l=(\varphi_{l,1},\varphi_{l,2})^T.$$

Then we consider the equation

$$\frac{d}{dt}Au^2=Lu^2+G(u^1,u^1),\qquad \lim_{t\to-\infty}u^2(x,y,t)=0,$$

from which we get

$$u^2=\sum_{j,k=1}^{4}\eta_j\eta_k e^{(\lambda_j+\lambda_k)t}e^{i(m_j+m_k)\alpha y}\phi_{jk}(x),$$

where ϕ_{jk} are the solutions of the following 1D ODE linear nonhomogeneous equation

$$\left[(\lambda_j+\lambda_k)A_{m_j+m_k}-L_{m_j+m_k}\right]\phi_{jk}=G_{m_j,m_k}(\varphi_j(x),\varphi_k(x)),\tag{5.16}$$

in which the operators A_m and L_m are defined by (3.4). Hence, the quadratic approximation of the center manifold becomes

$$h_2(x,y)=u^2|_{t=0}=\sum_{j,k=1}^{4}\eta_j\eta_k\Phi_{jk}(x,y),\tag{5.17}$$

where

$$\Phi_{jk}(x,y)=e^{i(m_j+m_k)\alpha y}\phi_{jk}(x).\tag{5.18}$$

Denote

$$g_{i,jk,l}=(G(\psi_i,\Phi_{jk})+G(\Phi_{jk},\psi_i),\psi_l^*),$$

the reduced equations (5.15) become

$$\begin{aligned}\frac{\partial\eta_1}{\partial t}&=\lambda_1\eta_1+\sum_{i,j,k=1}^{4}g_{i,jk,1}\eta_i\eta_j\eta_k+o(|\eta|^3),\\ \frac{\partial\eta_2}{\partial t}&=\lambda_2\eta_2+\sum_{i,j,k=1}^{4}g_{i,jk,2}\eta_i\eta_j\eta_k+o(|\eta|^3).\end{aligned}\tag{5.19}$$

Using (5.12) and (5.18), we find that

$$m_i + m_j + m_k - m_l \neq 0 \implies g_{i,jk,l} = 0,$$

which implies that the coefficients of the reduced equations (4.4) are

$$\begin{aligned} A &= g_{1,13,1} + g_{1,31,1} + g_{3,11,1}, \\ B &= g_{1,24,1} + g_{1,42,1} + g_{2,41,1} + g_{2,14,1} + g_{4,21,1} + g_{4,12,1}, \\ C &= g_{1,32,2} + g_{1,23,2} + g_{3,12,2} + g_{3,21,2} + g_{2,13,2} + g_{2,31,2}, \\ D &= g_{2,24,2} + g_{2,42,2} + g_{4,22,2}. \end{aligned} \tag{5.20}$$

5.4. Proof of Theorem 4.2

Step 1. *We will first prove that an S^3 attractor Σ bifurcates on $R > R^*$.*

By Lemma 4.2, we know that the equations (2.5)–(2.7) can be reduced to (4.4) in a small neighborhood of $(\eta_1, \eta_2, \mathrm{R}) = (0, 0, \mathrm{R}^*)$. To prove that an S^3 attractor Σ bifurcates on $\mathrm{R} > \mathrm{R}^*$, we only need to prove that $\mathbf{0}$ of (2.12) is locally stable at $R = R^*$. For this, it suffices to show that $\eta = 0$ is a locally asymptotically stable solution of (4.4) at $\mathrm{Re}(\lambda_n) = \mathrm{Re}(\lambda_{n+1}) = 0$.

To simplify the analysis we first make a change of variables

$$\eta_1(t) = \sqrt{\rho_1(t)}e^{i\gamma_1(t)}, \qquad \eta_2(t) = \sqrt{\rho_2(t)}e^{i\gamma_2(t)},$$

and

$$\mu_1 = \mathrm{Re}(\lambda_{n,1}), \qquad \mu_2 = \mathrm{Re}(\lambda_{n+1,1}),$$

so that the real parts of the equations (4.4) become

$$\begin{aligned} \dot{\rho_1} &= 2\rho_1(\mu_1 + \mathrm{Re}(A)\rho_1 + \mathrm{Re}(B)\rho_2 + O(\rho_1^2 + \rho_2^2)), \\ \dot{\rho_2} &= 2\rho_2(\mu_2 + \mathrm{Re}(C)\rho_1 + \mathrm{Re}(D)\rho_2 + O(\rho_1^2 + \rho_2^2)) \end{aligned} \tag{5.21}$$

where $\rho_1 \geq 0$, $\rho_2 \geq 0$. By rescaling the variables and the time,

$$\xi_1 = -\mathrm{Re}(A)\rho_1, \qquad \xi_2 = -\mathrm{Re}(D)\rho_2, \qquad \tau = 2t,$$

and defining $\theta = \frac{\mathrm{Re}(B)}{\mathrm{Re}(D)}$, and $\delta = \frac{\mathrm{Re}(C)}{\mathrm{Re}(A)}$ as in (4.5), the equations (5.21) become

$$\begin{aligned} \dot{\xi_1} &= \xi_1(\mu_1 - \xi_1 - \theta\xi_2 + O(\xi_1^2 + \xi_2^2)), \\ \dot{\xi_2} &= \xi_2(\mu_2 - \delta\xi_1 - \xi_2 + O(\xi_1^2 + \xi_2^2)). \end{aligned} \tag{5.22}$$

Note that due to our assumptions (4.6) and the fact that $\rho_1 \geq 0$, $\rho_2 \geq 0$, we have

$$\xi_1 \geq 0, \qquad \xi_2 \geq 0, \tag{5.23}$$

At $\mathrm{R} = \mathrm{R}^*$, $\mu_1 = \mu_2 = 0$ and the preceding equations reduce to

$$\begin{aligned} \dot{\xi_1} &= -\xi_1^2 - \theta\xi_1\xi_2 + O(|\xi|^3)), \\ \dot{\xi_2} &= -\delta\xi_2\xi_1 - \xi_2^2 + O(|\xi|^3)). \end{aligned} \tag{5.24}$$

From (5.24) we can deduce that

$$\frac{d}{dt}\left(-\frac{\delta}{\theta}\xi_1 + \xi_2\right) = \frac{\delta}{\theta}\xi_1^2 - \xi_2^2 + O(|\xi|^3)) < 0,$$

in a sufficiently small neighborhood of $(\xi_1, \xi_2) = (0, 0)$ since $\delta > 0$ and $\theta < 0$ by (4.6). Thus the preceding inequality and (5.23) imply that

$$(\xi_1, \xi_2) \to (0, 0), \qquad \text{as } t \to +\infty.$$

Step 2. *Now we will show that* (5.22) *bifurcates to at most three solutions.*

It is easy to see that the system (5.22) always has the following three fixed points on $\mu_1 > 0$ and $\mu_2 > 0$

$$E_0 = (0, 0), \quad E_1 = (\mu_1, 0), \quad E_2 = (0, \mu_2).$$

Moreover under the condition (4.6) and $\delta\mu_1 < \mu_2$, an additional fixed point

$$E_3 = \left(\frac{\theta\mu_2 - \mu_1}{\theta\delta - 1}, \frac{\delta\mu_1 - \mu_2}{\theta\delta - 1}\right) + O(|\mu^2|),$$

appears on $\mu_1 > 0$ and $\mu_2 > 0$.

Step 3. *Now we carry out the stability analysis of the solutions* E_i, $i = 1, 2, 3$.

The Jacobian matrix corresponding to (5.22) is given by

$$J(\xi_1, \xi_2) = \begin{pmatrix} \mu_1 - 2\xi_1 - \theta\xi_2 & -\theta\xi_1 \\ -\delta\xi_2 & \mu_2 - 2\xi_2 - \delta\xi_1 \end{pmatrix} + O(|\xi|^2). \tag{5.25}$$

The eigenvalues of $J(E_1)$ satisfy

$$\beta_{E_1}^{(1)} = -\mu_1 + O(|\mu|^2) < 0, \qquad \beta_{E_1}^{(2)} = \mu_2 - \delta\mu_1 + O(|\mu|^2) \begin{cases} > 0, & \mu_2 > \delta\mu_1, \\ < 0, & \mu_2 < \delta\mu_1. \end{cases}$$

Hence, E_1 is unstable (stable) for $\mu_2 > \delta\mu_1$ ($\mu_2 < \delta\mu_1$). E_2 is a saddle since the eigenvalues of $J(E_2)$ satisfy

$$\beta_{E_2}^{(1)} = -\mu_2 + O(|\mu|^2) < 0, \qquad \beta_{E_2}^{(2)} = \mu_1 - \theta\mu_2 + O(|\mu|^2) > 0.$$

Now suppose that $\delta\mu_1 < \mu_2$ so that E_3 is also bifurcated. The eigenvalues of $J(E_3)$ then satisfy

$$\beta_{E_3}^{(1)} + \beta_{E_3}^{(2)} = \frac{\mu_2 - \delta\mu_1 + \mu_1 - \theta\mu_2}{\delta\theta - 1} < 0,$$
$$\beta_{E_3}^{(1)}\beta_{E_3}^{(2)} = \frac{(\mu_2 - \delta\mu_1)(\mu_1 - \theta\mu_2)}{1 - \delta\theta} > 0,$$

which means that the real part of the eigenvalues of $J(E_3)$ is negative, i.e., E_3 is stable.

6. Numerical results

To determine the transition numbers governing our main theorems, the eigenvalue problem (3.3) has to be solved for the first critical eigenvectors, and the corresponding dual eigenvectors. As the 1D eigenvalue problem (3.3) cannot be solved exactly, numerical methods have to be used. For this purpose, we use a Legendre-Galerkin method according to which, the unknown fields are expanded using a basis of N polynomials, which are compact combinations of Legendre polynomials satisfying the four boundary conditions.

We refer to [33] for the details of the Legendre-Galerkin method and to [21] for its use in dynamical transition problems. For the convergence of the numerical scheme in our experiment, we find that $N = 100$ is sufficient. Once the eigenproblem is solved, an approximation of the center manifold can be obtained using (5.6) for the simple multiplicity case and (5.16) for the double multiplicity case. Finally, the transition numbers P for the single multiplicity case and a set

of parameters A, B, C, D for the double multiplicity case are obtained by using the formulas (5.11) and (5.20), respectively. After these numbers are computed, the type of transition and the spatio-temporal character of the transition states are examined by Theorem 4.1 and Theorem 4.2. In this section, we present the main outcomes from these numerical procedures. For sake of comparison, the parameters used in all of our simulations are similar to those in [7]. Namely, we consider the values $\gamma = 1/9,\ 1/3$, and $S = 0.0457, 0.7310,\ 1.2577$.

6.1. Transitions from a pair of simple complex conjugate eigenvalues

Theorem 4.1 shows that if the system (2.12) satisfies the PES condition (3.5) at the critical value $R = R^*$, the type of transition is determined by the sign of $P_1 = \mathrm{Re}P$ given by (5.11). The numerical results for P_1 are shown in Figure 6.1-Figure 6.3.

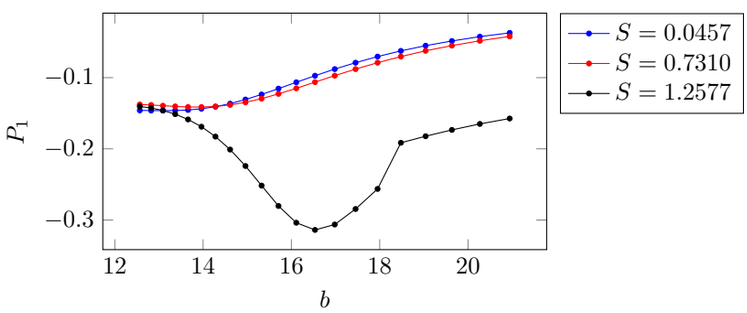

Figure 6.1: Transition number P_1 for $\gamma = 1/3$.

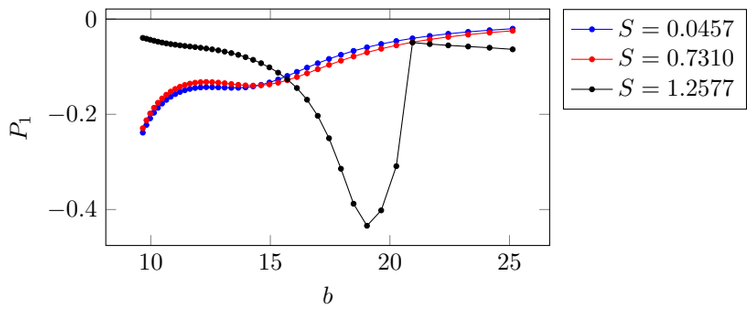

Figure 6.2: Transition number P_1 for $\gamma = 1/9$.

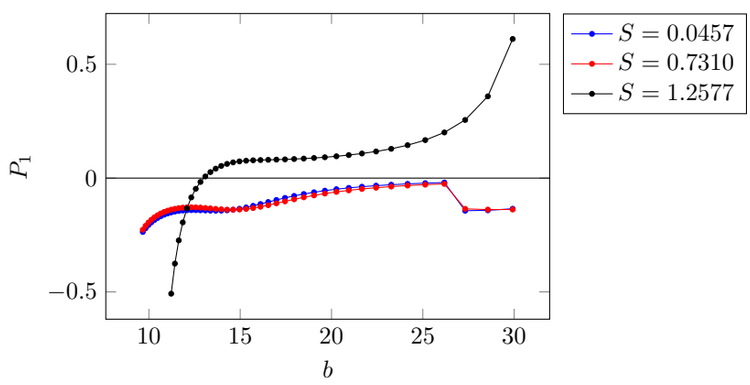

Figure 6.3: Transition number P_1 for $\gamma = 0$.

In all experiments, we found that the transition number P_1 is negative for the two-layer model ($\gamma \neq 0$), which dictates a continuous transition at the critical value $\mathrm{R} = \mathrm{R}^*$ as described by Theorem 4.1. Thus, a stable periodic solution describing the periodic circulation currents in the western boundary layer will emerge. This is in contrast with the single layer case ($\gamma = 0$), where the corresponding transition number can be positive for a large stratification number S (see Figure 6.3). It is not clear if the continuous transition is the only possible transition in the two-layer model ($\gamma \neq 0$), because we cannot rule out the possibility of jump transitions for different choices of parameters. If it is indeed the case that the two-layer model does not allow jump transitions, then a reason

behind this fact may follow from Figure 6.3, which suggests that a key factor leading to jump transition in the single layer case depends on the magnitude of the stratification number S, i.e., a larger stratification number favoring jump transitions. For the two-layer case, one can see from (2.5)–(2.7) that the stratification numbers for the upper layer and the lower layer currents are $S/(1+\gamma)$ and $S\gamma/(1+\gamma)$, respectively. Therefore, the stratification numbers cannot be large for both layers at the same time when $\gamma \neq 0$ is small. Consequently, a sudden change of the flow in one of the layers due to high stratification number may be restrained by the smallness of the stratification number of the flow in the other layer by some mechanisms that are not currently known.

In the case of a continuous transition obtained in our numerical experiments, the bifurcated stable time-periodic disturbance $\psi(x, y, t)$ of the basic profile, which is given by (4.3), has a spatial structure presented in Figure 6.4(a,b). The spatial structure of the stable bifurcated time-periodic solution given by $(\psi_s(x), 0) + \psi(x, y, t)$ is shown in Figure 6.4(c,b). The upper layer of this bifurcated solution is basically a small oscillation around the Munk profile $\psi(x)$, which exhibits typical boundary layer characteristics of the western boundary currents. Given the maximum velocity of the Munk profile is $\|v_s\|_\infty = 0.4731$, we can choose the characteristic length and time respectively as

$$(\nu/\beta_0)^{\frac{1}{3}} \sim 0.2 \times 10^5 m, \qquad (\nu/\beta_0)^{\frac{2}{3}} / \Psi_0 \sim 10^5 s. \tag{6.1}$$

The critical Reynolds number $\mathrm{R}^* = \Psi_0/\nu \approx 27.8$ corresponds to a critical characteristic velocity of $\Psi_0 \, (\beta_0/\nu)^{\frac{1}{3}} \, v_s \sim 0.1 m/s$, where Ψ_0 and ν are approximately given by $\Psi_0 \sim 10^5/25$, $\nu = 10^4/62$. The parameters above correspond to a basin size of about

$$L_x = (\nu/\beta_0)^{\frac{1}{3}} * a \sim 1000 km, \qquad L_y = (\nu/\beta_0)^{\frac{1}{3}} * b \sim 800 km,$$

and a time period of

$$T_r = T * (\nu/\beta_0)^{\frac{2}{3}} / \Psi_0 = 80.0108 \times 10^5 s \sim 92 \text{ days},$$

for the periodic solution shown in Figure 6.4(c,b).

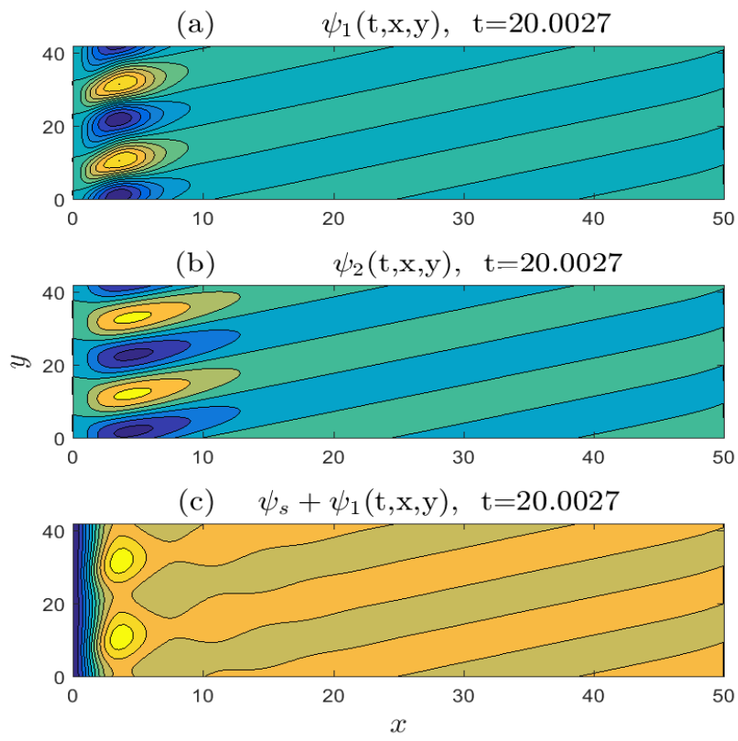

Figure 6.4: The bifurcated periodic solution with $a = 50,\ b = 40\pi/3,\ S = 0.1,\ \gamma = 1/9$ and $\mathrm{R} = 28.794 > \mathrm{R}^* = 27.794$ at a quarter of period $T/4 = 20.0027$.

6.2. Transitions from a double pair of simple complex conjugate eigenvalues

When the system (2.5)–(2.7) satisfies the PES condition (3.6), i.e. the first critical eigenvalues at the critical value $\mathrm{R} = \mathrm{R}^*$ have multiplicity four, the type of transition is determined by the sign of the real parts of A and D given by (5.20). For simplicity, let us denote

$$A = A_1 + iA_2, \qquad B = B_1 + iB_2,$$
$$C = C_1 + iC_2, \qquad D = D_1 + iD_2.$$

In Table 1, we first compute the critical wave number α and R^* for given γ and S so that the PES condition (3.6) holds. Next we compute the coefficients A, B, C, D of (4.4) given by (5.20). The numerical results given in Table 1 imply that the for the parameters we consider, the conditions (4.6), under which Theorem 4.2 is valid, are satisfied. Thus, we deduce that the system (2.5)–(2.7) also undergoes a continuous transition at the critical value and bifurcates to an S^3 attractor. According to Theorem 4.2, this S^3 attractor either contains both a stable and an unstable limit cycle, or it contains two unstable limit cycles and an attracting invariant torus. Moreover, both scenarios are realized as we show below.

For $\alpha = 0.24088297$, $S = 0.1$, $a = 50$, $\gamma = \frac{1}{9}$ and $\mathrm{R}^* = 30.5814$, we numerically obtain that the PES condition (3.6) is satisfied with $n = 1, 2$. When $\mathrm{R} = 31.5814$, we find that $\mathrm{Re}\,\lambda_{1,1} = 0.0006$ and $\mathrm{Re}\,\lambda_{2,1} = 0.0008$. Thus, we see that $\delta\,\mathrm{Re}\,\lambda_{n,1} > \lambda_{n+1,1}$, and the first scenario in Theorem 4.2 holds. Namely, the bifurcated S^3 attractor contains two periodic orbits, and the stable periodic one is ψ_{P2} whose spatial structure is similar to that in Figure 6.4.

For $\alpha = 0.15484982$, $S = 0.5$, $a = 50$, $\gamma = \frac{1}{9}$ and $\mathrm{R}^* = 34.9260$, it is seen that the PES condition (3.6) is satisfied with $n = 2, 3$. For slightly supercritical Reynolds number $\mathrm{R} = 35.9260$, we find that $\mathrm{Re}\,\lambda_{4,1} = 0.00054$, $\mathrm{Re}\,\lambda_{5,1} = 0.00044$, and $\delta\,\mathrm{Re}\,\lambda_{n,1} < \lambda_{n+1,1}$. Thus, the second scenario given in Theorem 4.2 holds. Namely, the bifurcated S^3 attractor contains two periodic orbits and a torus, which is the orbit of the quasi-periodic solution ψ_{P3}. The spatial structure of the quasi-periodic solution ψ_{P3} is shown in Figure 6.5(a,b), and that of $(\psi_s, 0) + \psi_{P3}$ is shown in Figure 6.5(c,b).

α	S	n	R^*	A_1	B_1	C_1	D_1
0.07822921	0.1	4(5)	27.5309	-0.0664	0.0296	-0.0261	-0.1285
0.08196955	0.3	4(5)	31.1888	-0.1418	0.0423	-0.0291	-0.0386
0.14166315	0.1	2(3)	28.2739	-0.0457	0.0601	-0.0310	-0.0825
0.10075159	0.1	3(4)	27.7412	-0.0583	0.0420	-0.0276	-0.1143
0.14896753	0.3	2(3)	32.4161	-0.1074	0.0701	-0.0399	-0.0215
0.10566779	0.3	3(4)	31.5270	-0.1321	0.0556	-0.0321	-0.0281
0.15484982	0.5	2(3)	34.9260	-0.1654	0.0595	-0.0492	-0.0126
0.10973110	0.5	3(4)	33.5955	-0.1676	0.0509	-0.0380	-0.0135
0.24088297	0.1	1(2)	30.5814	-0.0248	0.0768	-0.0422	-0.0544
0.25581456	0.3	1(2)	36.7237	-0.0596	0.0568	-0.0687	-0.0342
0.26398003	0.5	1(2)	41.1021	-0.0949	0.0601	-0.0917	-0.0273
0.27285168	0.7	1(2)	43.3022	-0.1367	0.0784	-0.1078	-0.0243
0.28442682	0.9	1(2)	43.1798	-0.1980	0.1113	-0.1119	-0.0299

Table 1: Coefficients of the reduced equation (4.4), $\gamma = 1/9$ and various S at the critical value $\alpha = 2\pi/b$.

Table 2 also suggests that for small aspect ratio ($b < 40$ or $\alpha > 0.16$), $n = 1$ and the condition $\delta \operatorname{Re} \lambda_{n,1} > \operatorname{Re} \lambda_{n+1,1}$ holds true. In this case a periodic oscillation around the Munk profile becomes stable as discussed previously. However for larger aspect ratios, $n > 1$ and the condition $\delta \operatorname{Re} \lambda_{n,1} < \operatorname{Re} \lambda_{n+1,1}$ holds true, where the new stable state after the transition is the quasi-periodic solution.

α	S	n	R^*	R	$\lambda_{n,1}(R)$	$\lambda_{n+1,1}(R)$	$\delta\mu_1 - \mu_2$
0.07822921	0.1	4(5)	27.5309	28.5309	0.0008	0.0009	-0.0005
0.08196955	0.3	4(5)	31.1888	32.1888	0.0005	0.0006	-0.0004
0.14166315	0.1	2(3)	28.2739	29.2739	0.0007	0.0009	-0.0004
0.10075159	0.1	3(4)	27.7412	28.7412	0.0008	0.0009	-0.0005
0.14896753	0.3	2(3)	32.4161	33.4161	0.00056	0.0006	-0.0003
0.10566779	0.3	3(4)	31.5270	32.5270	0.00057	0.00061	-0.0004
0.15484982	0.5	2(3)	34.9260	35.9260	0.00054	0.00044	-0.0002
0.10973110	0.5	3(4)	33.5955	34.5955	0.00052	-0.00047	-0.0003
0.24088297	0.1	1(2)	30.5814	31.5814	0.0006	0.0008	0.0001
0.25581456	0.3	1(2)	36.7237	37.7237	0.0006	0.0005	0.00018
0.26398003	0.5	1(2)	41.1021	42.1021	0.00058	0.00033	0.0002
0.27285168	0.7	1(2)	43.3022	44.3022	0.00058	0.00026	0.00017
0.28442682	0.9	1(2)	43.1798	44.1798	0.00056	0.00024	0.00005

Table 2: Parameters used to numerically predict the scenarios given in Theorem 4.2 with control parameters $\gamma = 1/9$, and various S and $\alpha = 2\pi/b$.

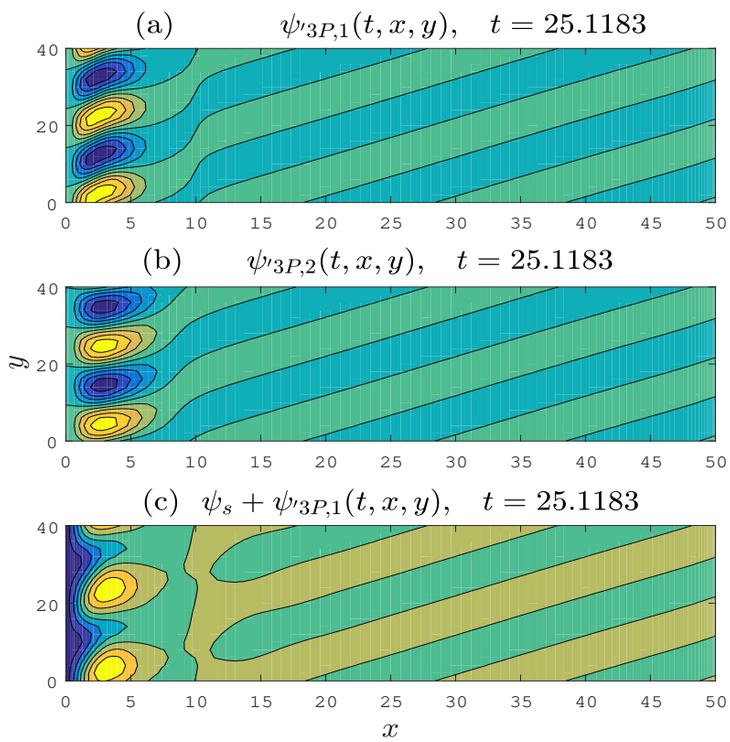

Figure 6.5: The bifurcated stable solution with $(n = 2, 3)$ $\alpha = 0.15484982$, $S = 0.5$, $\gamma = 1/9, \mathrm{R} = 35.9260 > \mathrm{R}^* = 34.9260$

6.3. Conclusions

The western boundary currents are an important feature of the oceanic dynamics whose underlying physical mechanisms are not well understood. Previous modelling studies of the western boundary currents showed the existence of two distinct mechanisms leading to the circulation: the viscous instability [4, 7, 19] driven by the Reynolds number R, and the wind-driven instability [5, 7, 9, 13, 14, 18] driven by the intensity of the wind. The focus in these studies has been so far mostly on the purely numerical simulations for the one-layer or two-layer models using the finite differences method or the trigonometric

series expansion. By specifying the control parameters in these models, these studies could obtain some results associated with the instability and bifurcation [4, 7, 9, 13, 14, 18]. Some of these previous studies also dealt with the linear stability of the steady-states including the Munk profile [7, 19] by numerically solving the Orr-Sommerfeld equation with the second-order finite differences.

Although the previous studies on WBCs could provide some insight into the GOSC behaviors and numerically demonstrate the existence of a critical parameter above which the initial steady flow (such as the Munk profile) is unstable, they lack the dynamical analyses for different critical parameters. The main difficulty in the dynamical analysis of the WBC problem roots in the derivation of the reduced equations (4.2) and (4.4) at the critical control parameter. In this work, we first presented a reduced equation on the central manifold by employing a technique that allows for the second-order approximation of the corresponding center manifold function. These techniques are entirely different from that used in the previous studies [20, 22, 23, 24, 25, 26]. Our method is easier to understand, and can also be used to derive high order approximation of the corresponding center manifold function. The reduced equations (4.2) and (4.4) are valid if and only if the assumption (3.1) holds true.

To examine the assumption (3.1) and solve the critical Reynolds number R^*, we used a Legendre-Galerkin method to find the corresponding eigenvalue problems, and then estimated the coefficients in the reduced equations (4.2) and (4.4). After numerically verifying the assumption (3.1) and obtaining the reduced equations (4.2) and (4.4), we addressed the instability problem from the perspective of the dynamic transition theory developed by Ma and Wang [20] which is different from previous research. Our results showed that the Reynolds number R indeed plays an important role in the formation of the oceanic circulation in the western boundary layer. From the perspective of dynamic transition theory, there exists a critical Reynolds number R^* above which there is a good transition of the Munk profile in the sense that it will be gradually replaced by a new motion. Usually the new motion is a unique time periodic motion, which may correspond to the actual circulation in the western boundary layer. How-

ever, for some critical aspect ratios of the domain, Theorem 4.2 shows that the emerging circulation is non-unique and has a complicated temporal behavior, because all possible asymptotic states form an attractor homeomorphic to a 3D sphere comprising of periodic and quasi-periodic motions and the transitions between them.

Our results also show that the two-layer western boundary currents model differs from the single-layer western boundary current model. In the one-layer model ,which is equivalent to $\gamma = 0$ in two layer model, the corresponding transition can be catastrophic at the critical R^*. That is for $0 < \frac{R-R^*}{R} \ll 1$, there is no stable periodic motion bifurcated from the Munk profile, while for $R < R^*$, the state of motion will jump from the Munk profile to another state and there exists a singular separation, i.e there exists a sudden change in state of motion in WBCs. As a result, the one-layer model has nondeterminacy for a real western boundary layer current due to the existence of the catastrophic transition. In a more realistic simulation, the choice of the model must be relied on the real control parameters and the scaling of the motion to determine which model can more accurately describe the motion of western boundary layer currents.

Acknowledgments This research was partially supported by the NOAA HFIP funding (Award NA16NWS4680026), the Vice Provost for Research through the Indiana University Faculty Research Support Program, and the IU Grant Challenge. We thank two anonymous reviewers for their constructive comments and suggestion.

References

[1] J. G. Charney, The gulf stream as an inertial boundary layer, Pro. Natl. Acad. Sci. 41 (1955) 731–740.

[2] H. Stommel, The Gulf Stream: A Physical and Dynamical Description, California library reprint series. University of California Press, 1965.

[3] L. Stramma, J. R. E. Lutjeharms, The flow field of the subtropical gyre of the south indian ocean, J. Geophy. Res.: Oceans 102 (C3) (1997) 5513–5530.

[4] K. Bryan, A numerical investigation of nonlinear model of wind-driven ocean, J. Atmos. Sci. 20 (1963) 594–606.

[5] V. M. Kamenkovich, S. O. Beloyserkovskii, M. C. Panteleev, On the problem of numerical modeling a barotropic current generated by a large scale wind field, Izv. POLYMODE 15 (1985) 3–23.

[6] M. C. Panteleev, Then influence of friction on the character of the barotropic wind driven circulation, Izv. POLYMODE 15 (1985) 34–39.

[7] P. Berloff, S. Meacham, On the stability of the wind-driven circulation, J. Mar. Res. 56 (5) (1998) 937–993.

[8] M. Ghil, The wind-driven ocean circulation: applying dynamical systems theory to a climate problem, Discrete Contin. Dyn. Syst. 37 (1) (2017) 189–228.

[9] E. Simonnet, M. Ghil, K. Ide, S. Wang, Low-frequency variability in shallow-water models of the wind-driven ocean circulation. part i: Steady-state solution, J. P. O. 33 (2003) 712–728.

[10] J. Pedlosky, Hydrodynamic and hydromagnetic stability, Springer, Second Edition, 1987.

[11] H. Stommel, The westward intensification of wind-driven ocean currents, Eos 29 (1948) 202–206.

[12] W. H. Munk, On the wind-driven ocean circulation, Journal of Meteorology 7 (2) (1950) 80–93.

[13] G. Veronis, Wind-driven ocean circulation: Part 1. linear theory and perturbation analysis, Deep-Sea Research 13 (1) (1966) 17 – 29.

[14] G. Veronis, Wind-driven ocean circulation: Part 2. numerical solutions of the non-linear problem, Deep-Sea Research 13 (1) (1966) 31 – 55.

[15] B. S. Attili, Numerical treatment of singularly perturbed two point boundary value problems exhibiting boundary layers, Commun. Nonlinear Sci. Numer. Simul. 16 (9) (2011) 3504–3511.

[16] Q. Wang, Boundary layer separation of 2-d incompressible dirichlet flows, Discrete Contin. Dyn. Syst.-B 20 (2) (2015) 675–682.

[17] H. Luo, Q. Wang, T. Ma, A predicable condition for boundary layer separation of 2-d incompressible fluid flows, Nonlinear Anal. Real World Appl. 22 (2) (2015) 336–341.

[18] E. Simonnet, M. Ghil, K. Ide, S. Wang, Low-frequency variability in shallow-water models of the wind-driven ocean circulation. part i: Steady-state solution, J. P. O. 33 (2003) 729–752.

[19] G. R. Ierley, W. R. Young, Viscous instabilities in the western boundary layer, J. Phys. Oceanogr. 21 (9) (1991) 1323–1332.

[20] T. Ma, S. Wang, Phase transition dynamics, Springer, 2014.

[21] H. Dijkstra, T. Sengul, J. Shen, S. Wang, Dynamic transitions of quasi-geostrophic channel flow, SIAM J. Appl. Math. 75 (5) (2015) 2361–2378.

[22] T. Ma, S. Wang, Rayleigh-Bénard convection: dynamics and structure in the physical space, Commun. Math. Sci. 5 (3) (2007) 553–574.

[23] T. Sengul, S. Wang, Pattern formation in Rayleigh-Bénard convection, Commun. Math. Sci. 11 (1) (2013) 315–343.

[24] T. Sengul, J. Shen, S. Wang, Pattern formations of 2D Rayleigh-Bénard convection with no-slip boundary conditions for the velocity at the critical length scales, Math. Methods Appl. Sci. 38 (17) (2015) 3792–3806.

[25] H. Liu, T. Sengul, S. Wang, Dynamic transitions for quasilinear systems and Cahn-Hilliard equation with Onsager mobility, J. Math. Phys. 53 (2) (2012) 023518, 31.

[26] H. Liu, T. Sengul, S. Wang, P. Zhang, Dynamic transitions and pattern formations for a Cahn-Hilliard model with long-range repulsive interactions, Commun. Math. Sci. 13 (5) (2015) 1289–1315.

[27] T. Ma, S. Wang, Boundary-layer and interior separations in the Taylor-Couette-Poiseuille flow, J. Math. Phys. 50 (3) (2009) 033101, 29.

[28] Q. Wang, Stability and bifurcation of a viscous incompressible plasma fluid contained between two concentric rotating cylinders, Discrete Contin. Dyn. Syst.-B 19 (2) (2014) 543 – 563.

[29] S. Ozer, T. Sengul, Stability and transitions of the second grade Poiseuille flow, Phys. D 331 (2016) 71 – 81.

[30] A. Majda, X. Wang, Nonlinear dynamics and statistical theories for basic geophysical flows, Cambridge University Press, 2006.

[31] D. Henry, Geometric theory of semilinear parabolic equations, Vol. 840, Springer, 2006.

[32] Y. A. Kuznetsov, Elements of applied bifurcation theory, Vol. 112, Springer Science & Business Media, 2013.

[33] J. Shen, T. Tang, L.-L. Wang, Spectral methods: algorithms, analysis and applications, Vol. 41, Springer Science & Business Media, 2011.